An efficient virtual crystal approximation that can be used to treat heterovalent atoms, applied to $(1-x)BiScO_3-xPbTiO_3$

2007 J. Phys.: Condens. Matter 19 306203

(http://iopscience.iop.org/0953-8984/19/30/306203)

IOP PUBLISHING JOURNAL OF PHYSICS: CONDENSED MATTER

J. Phys.: Condens. Matter **19** (2007) 306203 (13pp) doi:10.1088/0953-8984/19/30/306203

An efficient virtual crystal approximation that can be used to treat heterovalent atoms, applied to $(1-x)BiScO_3$–$xPbTiO_3$

Chol-Jun Yu[1,2] **and Heike Emmerich**[1]

[1] Computational Materials Engineering, Institute of Minerals Engineering, RWTH Aachen University, D-52064 Aachen, Germany
[2] Natural Science Centre, Kim Il Sung University, Ryongnam-Dong, Taesong-District, Pyongyang, DPR Korea

E-mail: yucj@ghi.rwth-aachen.de

Received 26 March 2007, in final form 27 March 2007
Published 11 July 2007
Online at stacks.iop.org/JPhysCM/19/306203

Abstract

It is well accepted that the virtual crystal approximation provides an effective method for studying solid solutions and alloys from first principles. Here we propose another approach based on a well designed averaging of the pseudo-wavefunctions. As from physical and numerical considerations there is a subtle arbitrariness in constructing the Kleinman–Bylander pseudopotential, we can construct the orthonormalized pseudo-wavefunctions as well as pseudopotentials of the virtual atom by averaging. It is proved that this extended averaging approach can provide reasonable properties for heterovalent solid solutions, and has the advantage of great simplicity. Our results for the perovskite ferroelectrics $(1-x)BiScO_3$–$xPbTiO_3$ satisfy Vegard's law well as regards the cubic lattice constants and display improved values as regards the structural and electrical properties compared with a previous work (Íñiguez *et al* 2003 *Phys. Rev.* B **67** 224107).

(Some figures in this article are in colour only in the electronic version)

1. Introduction

The material properties of solid solutions and alloys have been widely studied both experimentally and theoretically throughout materials science. In particular, ferroelectric ceramics correspond to a typical materials class for which most of the realistic applications are implemented with solid solutions. For treating such materials systems within first-principles methods, there exist two approaches: the supercell (SC) method and the virtual crystal approximation (VCA) method. Firstly, it is necessary to mention the advantages and

shortcomings of both methods. The former can give more correct results but require more computational resources compared with the latter. The issue of correctness is related to the fact that the SC method can describe the local interaction between two atoms which consist of virtual atoms but the VCA method cannot do that. It is clear that the effectiveness of the calculation is connected with the fact that the supercell may contain many unit cells unlike the primitive unit cell of the VCA method. In the year 2000, several modern VCA approaches were developed with their own advantages and shortcomings. Here mainly two issues are considered: capability for treating the heterovalent atoms and accuracy of the calculation.

Let us consider such approaches simply. The simplest VCA approach will be the simple mixing of the pseudopotentials [1, 2]. In practice, this is performed through the averaging of the matrix elements in reciprocal space (Fourier momentum space). The advantage is the simplicity but it is not sufficiently accurate in some cases. The reason for the incorrectness is the mixing of only the potentials. Ramer and Rappe [1] developed a more accurate VCA approach through performing the averaging at the level of atomic calculation, where the averagings of eigenvalues of valence orbitals, Coulomb nuclear potentials, core charge densities and wavefunctions are performed. The shortcoming of this method is not being applicable for treating heterovalent atoms; the method only creates the pseudopotential of the virtual atom composed of homovalent atoms. The weighted averaging method of Bellaiche and Vanderbilt [3] provides further capability for realizing an effective VCA approach. Its advantages are providing the ability to treat the heterovalent system and generality for application to all kinds of first-principles pseudopotentials. However, this method can be considered also as a kind of simple mixing of pseudopotentials in the case of the norm-conserving types, though the additional averaging process (with respect to a kind of wavefunction, $Q(r)$), is performed in the case of the ultrasoft pseudopotential. Therefore, the resulting values in the case of complex heterovalent systems [17] show small deviation from the SC and the experimental values.

Through the simple explanation of the previous VCA approaches we can find that the accuracy of the calculation improves according to the level of averaging: more averaging can provide more reasonable results. Here it is necessary to carefully consider the procedure of constructing the Kleinman–Bylander (KB) [4, 5] nonlocal separable pseudopotential, in the form of which the pseudopotentials [6–11] are generally used. Transformation from the semi-local into the KB nonlocal pseudopotential is performed by adopting angular momentum dependent nonlocal projectors, which in principle may be an arbitrary complete set of functions. Usually the pseudo-wavefunctions of isolated pseudo-atoms are used as such a set of functions [12–14]. To avoid the problem of ghost states and to improve the transferability, a multiple-projector formalism has been developed [15, 16]. In this context it is essential to realize that an arbitrary set of functions can be used for constructing a KB pseudopotential, except for the condition that the set is complete and orthonormalized.

On the basis of the above consideration we propose an approach where the pseudo-wavefunctions as well as the ionic pseudopotential of pseudo-atoms are averaged, imposing the norm-conserving condition of the averaged wavefunctions. We demonstrate that this approach allows us to solve the previously encountered difficulty in treating heterovalent atoms in the Ramer and Rappe approach with reasonable results. And also this approach has the advantage that it is very simple to apply. Since our new method extends the simple approach of averaging for only potentials to the averaging for both potentials and wavefunctions, we call it the '*Yu–Emmerich extended averaging approach*', for short YE^2A^2. We test the validity of the YE^2A^2 via an application to the structural, electronic, electrical and elastic properties of $(1-x)BiScO_3$–$xPbTiO_3$ (BS–PT) investigated in previous work [17] by means of the weighted averaging VCA.

We organize our paper as follows. In section 2, the main formalism of our new approach is given. Section 3 shows the results of its application to BS–PT. Finally, we summarize our results in section 4.

2. Main formalism

The first step consists in performing all-electron calculations for the isolated atoms. From this one obtains the all-electron potential, wavefunctions and eigenvalues, which are required for constructing the norm-conserving pseudopotential. Afterwards the pseudo-wavefunctions and the semi-local pseudopotentials are generated from the all-electron quantities.

The next step is the averaging of the descreened angular momentum (l) dependent ionic pseudopotentials,

$$V_l^{\mathrm{ion,VA}}(r) = x\,V_l^{\mathrm{ion,A}}(r) + (1-x)\,V_l^{\mathrm{ion,B}}(r), \tag{1}$$

where $V_l^{\mathrm{ion,A}}(r)$, $V_l^{\mathrm{ion,B}}(r)$ and $V_l^{\mathrm{ion,VA}}(r)$ are l components of the ionic pseudopotentials of atom A, atom B and the virtual atom $\mathrm{A}_x\mathrm{B}_{1-x}$, respectively [1, 2].

When these ionic pseudopotentials are used in calculations of polyatomic systems such as solids and molecules, they are transformed into sums of an l independent local part and l dependent nonlocal parts. In the semi-local formalism, the pseudopotential operator is written as follows:

$$\widehat{V}^{\mathrm{PP}} = V^{\mathrm{loc}}(r) + \sum_l \Delta V_l^{\mathrm{nl}}(r)\,\widehat{P}_l, \tag{2}$$

where $V^{\mathrm{loc}}(r)$ is a local pseudopotential, $\Delta V_l^{\mathrm{nl}}(r) = V_l^{\mathrm{ion}}(r) - V^{\mathrm{loc}}(r)$ are nonlocal pseudopotentials and $\widehat{P}_l$ are projection operators, which pick out the lth component from the subsequent wavefunction. The pseudopotential operator $\widehat{V}^{\mathrm{PP}}$ is a semi-local operator in the sense that it is local with respect to the radial coordinate r, but nonlocal with respect to the angular coordinates $\hat{\mathbf{r}}$.

In the KB formalism, the pseudopotential operator can be written in a fully nonlocal representation as follows:

$$\widehat{V}^{\mathrm{PP}} = V^{\mathrm{loc}}(r) + \sum_{i,j} |\alpha_i\rangle B_{ij} \langle\alpha_j|, \tag{3}$$

where $\alpha_i(\mathbf{r})$ are suitably chosen projection functions which are strictly localized within the core cut-off radius and B is the real matrix. We show the detailed transformation of the semi-local pseudopotential into the fully nonlocal pseudopotential in the appendix[3]. Kleinman and Bylander proposed that the pseudo-wavefunctions, $\psi_{lm}^0(\mathbf{r}) = R_l^0(r)Y_{lm}(\hat{\mathbf{r}})$, where $R_l^0(r)$ are radial wavefunctions and $Y_{lm}(\hat{\mathbf{r}})$ are spherical harmonics, can be used as a set of appropriate projection functions [4, 5], i.e.

$$\widehat{V}^{\mathrm{PP}} = V^{\mathrm{loc}}(r) + \sum_{lm} \frac{|\Delta V_l \psi_{lm}^0\rangle\langle\psi_{lm}^0 \Delta V_l|}{\langle\psi_{lm}^0|\Delta V_l|\psi_{lm}^0\rangle}. \tag{4}$$

At this point it is essential to understand that this expression for the projection functions remains an approximation, since $\widehat{V}^{\mathrm{PP}}\psi_{lm}^0 = V^{\mathrm{PP}}\psi_{lm}^0$ is valid for an isolated atom, but usually $\widehat{V}^{\mathrm{PP}}\psi \simeq V^{\mathrm{PP}}\psi$ for a polyatomic system[4]. However, the effect of this difference on the pseudo-wavefunctions can be assumed to be just a perturbation, so that the approximation is certainly a reliable one.

[3] Note that this construction is still fully along the lines of the KB formalism, which only requires the set of projection functions to be complete, orthonormalized and localized within the core cut-off radius.

[4] The reason for this is that the chemical environment of the latter differs from the one in an isolated atom.

Now equation (4) can be rewritten on the basis of the radial wavefunctions $R_l^0(r)$ as follows [12]:

$$\widehat{V}^{\mathrm{PP}} = V^{\mathrm{loc}}(r) + \sum_{lm} |\psi_{lm}^{\mathrm{KB}}\rangle E_l^{\mathrm{KB}} \langle \psi_{lm}^{\mathrm{KB}}|, \tag{5}$$

where the KB eigenvectors $\psi_{lm}^{\mathrm{KB}}(\mathbf{r})$ and KB energy E_l^{KB} are expressed as

$$\psi_{lm}^{\mathrm{KB}}(\mathbf{r}) = Y_{lm}(\hat{\mathbf{r}}) R_l^{\mathrm{KB}}(r) = Y_{lm}(\hat{\mathbf{r}}) \frac{\Delta V_l(r) R_l^0(r)}{\left[\int_0^\infty \mathrm{d}r\, r^2 |R_l^0(r)|^2 |\Delta V_l(r)|^2\right]^{1/2}}, \tag{6}$$

$$E_l^{\mathrm{KB}} = \frac{\int_0^\infty \mathrm{d}r\, r^2 |R_l^0(r)|^2 |\Delta V_l(r)|^2}{\int_0^\infty \mathrm{d}r\, r^2 |R_l^0(r)|^2 \Delta V_l(r)}. \tag{7}$$

As shown extensively in the literature, the pseudopotential matrix in momentum space can be designed such that the construction time and memory cost of the matrix can be reduced substantially. The matrix elements are then given as follows:

$$\langle \mathbf{K}|\widehat{V}^{\mathrm{PP}}|\mathbf{K}'\rangle = \frac{4\pi}{\Omega} \sum_l E_l^{\mathrm{KB}} P_l(\cos(\widehat{\mathbf{K}\mathbf{K}'})) \left[\int_0^\infty \mathrm{d}r\, f_K(r)\right] \left[\int_0^\infty \mathrm{d}r\, f_{K'}(r)\right] \tag{8}$$

where $\mathbf{K} = \mathbf{k} + \mathbf{G}$ and $f_K(r) = r^2 j_l(Kr) R_l^{\mathrm{KB}}(r)$. Moreover, $\mathbf{k}$ is a special point in the irreducible Brillouin zone, $\mathbf{G}$ is a lattice vector in reciprocal space, Ω is the volume of the unit cell, $\widehat{\mathbf{K}\mathbf{K}'}$ is the angle between wavevectors $\mathbf{K}$ and $\mathbf{K}'$, P_l is the lth Legendre polynomial and j_l is the lth spherical Bessel function.

Here we propose that the averaged pseudo-wavefunctions can be used as pseudo-wavefunctions of the virtual atom, as follows:

$$R_l'^{\mathrm{VA}}(r) = x R_l^{0,\mathrm{A}}(r) + (1-x) R_l^{0,\mathrm{B}}(r). \tag{9}$$

At this time, since the normalization condition of the wavefunctions is lost, we impose normalization on them as follows:

$$R_l^{\mathrm{VA}}(r) = \frac{R_l'^{\mathrm{VA}}(r)}{\left[\int_0^\infty \mathrm{d}r\, r^2 |R_l'^{\mathrm{VA}}(r)|^2\right]^{1/2}}. \tag{10}$$

Then, $R_l^0(r)$ in equations (6) and (7) has to be replaced by $R_l^{\mathrm{VA}}(r)$. The physical motivation for this is as follows. Since the Schrödinger equation is nonlinear with respect to the eigenfunctions, the linear combination of the eigenfunctions (R_l^{VA}) is not an exact eigenfunction of the linear combination of the potentials (V_l^{VA}). However, it is justified to assume the difference from the exact eigenfunction to be small. Moreover, the exact eigenfunctions of V_l^{VA} in the environment of an isolated virtual atom are actually no longer accurate ones when the virtual atom is put into a solid or a molecule. Therefore the linear combination of the pseudo-wavefunctions taking into account the mixing ratio should fit even better to the polyatomic environment than the exact eigenfunction of the virtual atom in an isolated environment.

$\mathrm{YE^2A^2}$ as outlined above has the advantage that it is easy to implement for heterovalent atoms because it does not require one to solve the Schrödinger equation for the virtual atom. When applying $\mathrm{YE^2A^2}$, note that the maximum angular momentum number $l_{\max}$ up to which the semi-local pseudopotentials are generated must be the same for all component atoms. Moreover, unbounded states must have the same l, as well. In *ab initio* calculations of solid solutions based on $\mathrm{YE^2A^2}$, the virtual atomic number of the virtual atom has to be averaged as $Z^{\mathrm{VA}} = xZ^{\mathrm{A}} + (1-x)Z^{\mathrm{B}}$, as well.

Table 1. Cubic lattice constants optimized and fitting into Murnaghan's state equation, where 'Ave.' means averaged value.

		Lattice constant (Bohr)		Murnaghan		
	x	Calc.	Ave.	a_0 (Bohr)	B_0 (Mbar)	B_0'
BS	0.00	7.611	7.611	7.615	6.635	5.194
0.75BS–0.25PT	0.25	7.575	7.567	7.563	7.054	5.905
0.5BS–0.5PT	0.50	7.520	7.523	7.517	7.412	4.655
0.25BS–0.75PT	0.75	7.485	7.480	7.484	7.556	4.757
PT	1.00	7.436	7.436	7.441	7.815	4.284

3. Application to BS–PT

The results that we present in this paper concern the electronic, structural, electrical and elastic properties of the perovskite piezoelectric solid solution bismuth scandinate–lead titanate, $(1-x)BiScO_3$–$xPbTiO_3$, which has already been investigated by means of both first-principles studies [17] and experiments [18, 19]. Since it was discovered recently, it has been proved that BS–PT single crystal near the morphological boundary (MPB) region possesses a significantly high Curie temperature and good piezoelectric properties. Because there are no applications to heterovalent systems via the first-principles VCA method except for BS–PT, we verify the validation of our improved VCA method through comparison with the previous work [17]. Moreover, we display the additional properties of BS–PT which were not mentioned there.

The construction of pseudopotentials is performed by using the Opium package[5], which adopts the optimized norm-conserving pseudopotential with the designed nonlocal potential approach suggested by Rappe *et al* [9]. Here two pairs of atoms, Bi–Pb and Sc–Ti, are considered as the virtual atoms. The Perdew–Zunger formalism [23] for the exchange–correlation functional within the local density approximation (LDA) is used. As stated in [17], Bi–Pb and Sc–Ti are pairs of neighbouring atoms in the periodic table and Bi–Sc and Pb–Ti pairs have the same total nominal ionic charge of 6+, allowing them to be mixed in arbitrary proportions. The valence electronic configurations of atoms used in this work are as follows: Bi: $5d^{10}$, $6s^2$, $6p^3$; Pb: $5d^{10}$, $6s^2$, $6p^2$; Sc: $3s^2$, $3p^6$, $3d^1$, $4s^2$; Ti: $3s^2$, $3p^6$, $3d^2$, $4s^2$; and O: $2s^2$, $2p^4$. The implementation for the crystals is performed by using ABINIT 5.2.4 [24] with the following parameters: cut-off energy 45 Hartree, Monkhorst–Pack special k-point sets $(4 \times 4 \times 4)$ for structural optimization, $(6 \times 6 \times 6)$ for dynamical calculation and $(4 \times 4 \times 10)$ for polarization calculation of the tetragonal phase by the Berry phase method. The structural relaxation is evolved until the residual force is smaller than 10^{-6} Hartree $Bohr^{-1}$.

3.1. Structural properties

Firstly we verify that Vegard's law with respect to the lattice constants is satisfied well. In the case of BS, due to the large difference of ionic radii of Bi and Sc, its cubic phase is very unstable so that the experimental value is not available, since we are not able to compare with the experimental values. Table 1 shows the results and the fitting into Murnaghan's state equation. From table 1, it is found that the lattice constants simulated via optimization satisfy Vegard's law within allowable error and the ones obtained by fitting into Murnaghan's state equation also agree with the law. Meanwhile the bulk moduli have properly averaged behaviour.

[5] Features of the Opium package: atomic structure calculation, generation of norm-conserving-type pseudopotentials and suitability for use in the ABINIT package via conversion into the fhi format, http://opium.sourceforge.net/index.html

Table 2. Lattice parameters of the tetragonal phase obtained by full optimization, where the relaxed atomic coordinates relative to the A site are shown in units of c. In the case of theoretical work, BS–PT was considered at $x = 0.5$.

	This work			Previous work[a]				Exp.	
					BS–PT				BS–PT[a]
	BS	BS–PT	PT	BS	(VCA)	(SC)	PT	PT[b]	($x = 0.64$)
a (Bohr)	7.182	7.415	7.373	7.113	7.244		7.293	7.373	
c (Bohr)	9.270	8.061	7.806	9.140	8.070		7.650	7.852	
$d = c/a$	1.291	1.087	1.059	1.285	1.114	1.079	1.049	1.065	1.023
z(B)	0.571	0.569	0.540	0.573	0.571		0.535	0.538	
$z(O_x, O_y)$	0.730	0.672	0.621	0.729	0.682		0.606	0.612	
$z(O_z)$	0.174	0.129	0.102	0.177	0.145		0.094	0.117	
ΔE (eV)	−1.725	−0.935	−0.659	−1.124	−0.376	−0.472	−0.060		

[a] Reference [17].
[b] Reference [21].

Then we get the optimized tetragonal lattice parameters, which include the relaxed atomic positions, lattice constants a and c or tetragonal ratio $d = c/a$. The calculated values are displayed in table 2, where BS–PT is considered at $x = 0.5$ and ΔE is the difference energy relative to the equilibrium cubic phase. In ABO_3-type perovskite, the relaxed atomic coordinates relative to the A site are shown in units of c. Note that the atoms are relaxed in the direction of the z axis in the tetragonal phase and the ideal cubic perovskite coordinates are $z(B) = 0.5$, $z(O_x, O_y) = 0.5$ and $z(O_z) = 0.0$. Our tetragonal ratio d (1.087) for BS–PT ($x = 0.5$) is rather better than the previous one (1.114), from the fact that the experimental value is 1.023 for $x = 0.64$. Moreover our value is very close to the SC one (1.079). The order of atomic relaxation is similar to the previous results. However the ΔEs are larger in magnitude than the previous values. These results suggest that the cubic perovskite structure is not a very natural one for BS, which is mentioned in the previous work.

3.2. Electronic properties

We calculate the band structure and density of states in the cubic lattice, where the lattice constants optimized in this work are used. Through the analysis of the band structure and density of states, we can find the fundamental role of the individual atoms in the structural instabilities. Such an explanation can be also provided through the valence electronic charge densities. Figure 1 shows the band structure near the band gaps from Γ to the X point. Through figure 1 we can find the proper averaging behaviour of the band structures. However the band gaps are not well averaged, as the previous works also mentioned. In some works [22], the line of band gaps in solid solution semiconductors is usually nonlinear with the concentration of the component. Through the band structures against the concentration, we can verify that the band structures of solid solutions calculated by using our approach are well averaged in the context of the overall tendency, except the band gaps.

We then observe the partial densities of states (PDOS), which are shown in figure 2. In the part under −20 eV, we can find that there are two peaks which originate from the B site atom 3s state and 3p state hybridizing with O 2s and 2p states. These energy of peaks go downward gradually as the mixing ratio x is increased. This shows that the role of the 3s and 3p electrons of B site atoms in the ferroelectric instability becomes gradually weaker as the concentration of PT is increased. In the interval (−25 eV, −5 eV), we find the two different facts that the band from O 2s is downward and the bands from the A site 6s and 5d states are upward, when

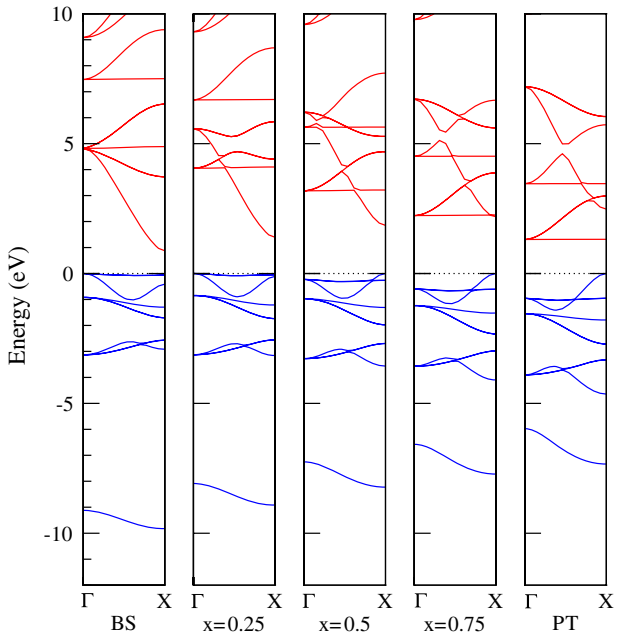

Figure 1. Band structure of the compounds near the band gaps from Γ to the X point.

the concentration of PT is increased. Consequently we can conclude that the role of 6s and 5d electrons of A site atoms becomes more important but 2s electrons of oxygen atoms weaken for the ferroelectric instabilities as the concentration of PT is increased. The most important part in this analysis is the detailed feature of the band gap region, (−10 eV, 10 eV). In the case of BS, we can find clearly that the hybridization between Bi 6p and O 2p orbitals plays a more important role in the ferroelectric instability than the hybridization between Sc 3d and O 2p orbitals, while in the case of PT the hybridization between Ti 3d and O 2p orbitals plays the role of instability. In other words, an A site metal atom plays an important role in the ferroelectric properties for BS, but the B site transition metal atom plays such a role for PT. Furthermore, we find the proper averaging characteristics between the PDOS of BS and PT in the solid solution BS–PT ($x = 0.5$).

In order to search for the change of charge densities as the concentration of PT is increased, we observe the line density in the directions [001] and [111] (figure 3). We find that the charge density around the A atoms is gradually decreased, but the charge density around the B atoms is increased, from BS to PT. This is reflected in the effective charge which is considered in the following section. The effect of the Bi atom on the chemical bond is stronger than that of the Pb atom, which was already mentioned in the analysis of band structures.

We emphasize that it is possible to calculate and analyse reasonable electronic properties of the solid solutions directly, while this is impossible or difficult in the cases of SC and weighted VCA.

3.3. Physical properties

On the basis of the fully optimized tetragonal lattices, we calculate the spontaneous polarizations, Born effective charge tensors, elastic tensors and piezoelectric tensors within modern density functional perturbation theory [25].

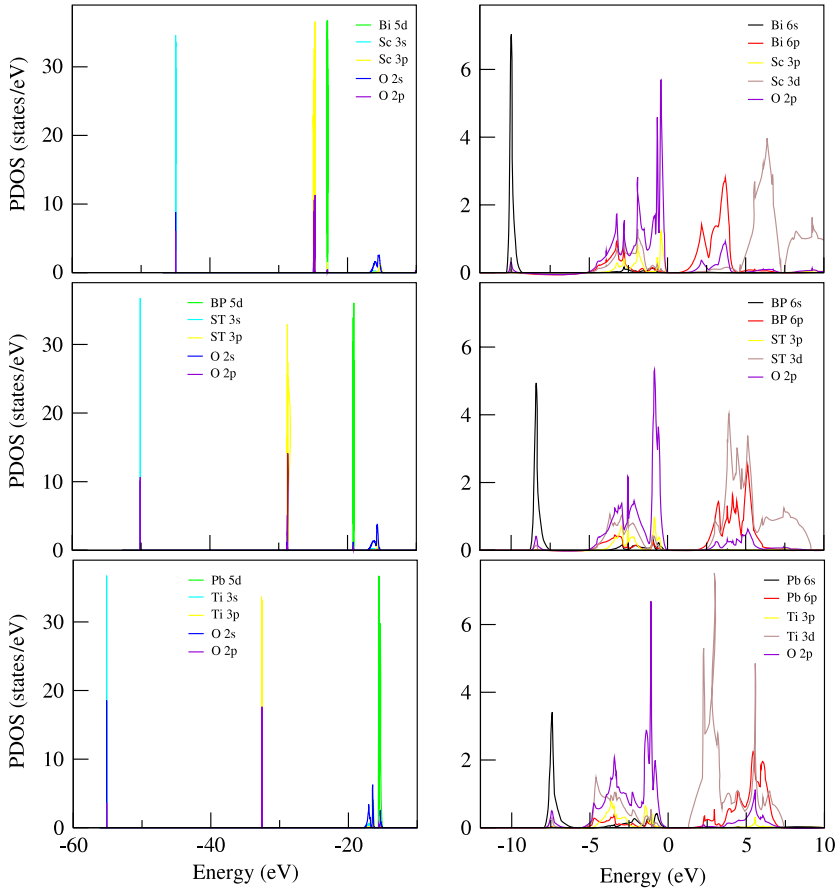

Figure 2. Partial DOS of BS (top panel), BS–PT0.5 (middle panel) and PT (bottom panel). In the middle panel BP and ST mean the pairs Bi–Pb and Sc–Ti.

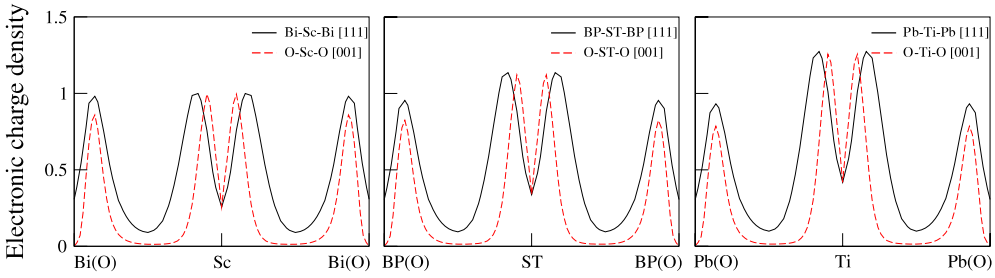

Figure 3. Electronic charge densities in the [001] and [111] directions of BS (left panel), BS–PT0.5 (middle panel) and PT (right panel).

The electronic part of the polarization can be calculated by the Berry phase method. It is well known that we can calculate the polarization difference between two states of the same solid, under the necessary condition that the crystal remains an insulator along the adiabatic path that transforms the two states into each other. The magnitude of the electronic polarization of a system in one state is defined only modulo ec/Ω, where c is the shortest real-space

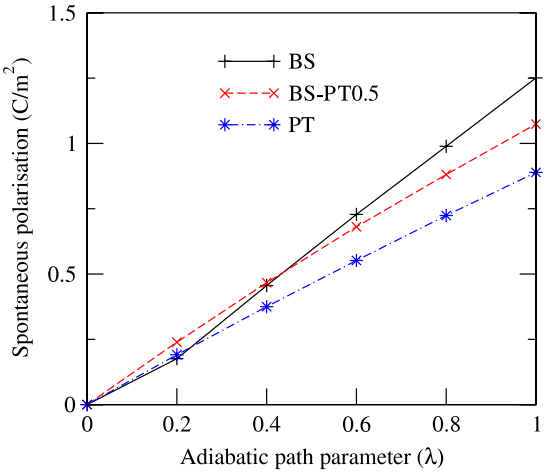

Figure 4. Polarizations on the adiabatic path.

Table 3. Spontaneous polarization (C m^{-2}).

	This work	Previous work	Exp.
BS	1.251	0.93[a]	—
0.5BS–0.5PT (VCA)	1.074	0.92 (VCA)[a]	0.32 ($x = 0.64$)[a]
		1.06(SC)[a]	0.74 (thin film)[b]
Average	1.070		
PT	0.889	0.82[c]	0.75[c]

[a] Reference [17].
[b] Reference [18].
[c] Reference [21].

lattice vector. The electronic polarization difference between two crystal states is expressed as $P^{\mathrm{el}} = P^{\mathrm{el}}(\lambda_2) - P^{\mathrm{el}}(\lambda_1)$. We calculated the polarizations along the adiabatic path via which the crystal transforms from the centrosymmetric state (atomic positions are not relaxed) to the ferroelectric state (atomic positions are relaxed) and estimated the differences between the centrosymmetric state and the ferroelectric relaxed state. Here the atomic positions of the intermediate states are estimated, like $x_\lambda = x_0 + \lambda(x_{\mathrm{relax}} - x_0); 0 < \lambda < 1)$, where λ is an adiabatic path parameter, x_0 is the position in the centrosymmetric state and x_{relax} is the relaxed position. Here the polarization differences along the adiabatic path should be linear. The linearity of the polarization differences along the adiabatic path is shown in figure 4. In figure 4, we also find good averaging behaviour of the BS–PT polarization differences between BS and PT.

Table 3 shows the spontaneous polarizations of the compounds. Our values for BS (1.251) and BS–PT (1.074) are larger than those from the previous work (0.93, 0.92) [17] but the averaging behaviour is good. Since the polarization is strongly dependent on the structure and our atomic relaxation is rather stronger than Vanderbilt's one, our larger values were already expected.

As mentioned previously, the largest contribution to the polarization comes from the displacement of Bi relative to its neighbouring O ions (O_x and O_y ions). We find that the relative displacement (0.159) of Bi in our work is a little larger than that from the previous work (0.146); see table 2. Here we emphasize that the polarization of BS–PT is very well

Table 4. The Born effective charge tensor in the tetragonal phase, where Z^*_{xx}/Z^*_{yy} means that $Z^*_{xx}(\mathrm{O}_x)$ is replaced with $Z^*_{yy}(\mathrm{O}_y)$ and vice versa.

	Z^*_{xx}/Z^*_{yy}					Z^*_{zz}				
	A	B	O_x	O_y	O_z	A	B	O_x	O_y	O_z
BS	5.72	3.26	−2.89	−3.34	−2.75	2.90	4.47	−1.99	−1.99	−3.38
BS–PT ($x = 0.5$)	4.82	4.73	−4.09	−3.03	−2.43	3.18	5.13	−2.07	−2.07	−4.17
Average	4.78	4.92	−4.21	−3.03	−2.46	3.16	5.03	−2.07	−2.07	−4.06
PT	3.83	6.58	−5.53	−2.72	−2.16	3.42	5.59	−2.14	−2.14	−4.73
BS[a]						2.90				
BS–PT ($x = 0.7$)[a]	4.26	5.27	−4.47	−2.77	−2.29					
PT[b]	3.74	6.20	−5.18	−2.61	−2.15	3.52	5.18	−2.16	−2.16	−4.38

[a] Reference [17].
[b] Reference [21].

averaged between BS and PT and moreover almost agrees with the SC value (1.06). Generally the experimental spontaneous polarization is measured for polycrystalline ceramics and the polarization of polycrystal is smaller than that of single crystal. Therefore it is necessary to establish a theorem for predicting the spontaneous polarization of the polycrystal from that of single crystal.

Next we consider the Born effective charge tensor of the compounds in table 4. Firstly we can confirm that the charge neutrality condition is also satisfied, $\sum_m Z^*_{\alpha\alpha}(m) = 0$, indicating that the calculations are relatively fully converged with respect to computational conditions. We observe that the averaging of the effective charges is reasonable, especially for the A virtual atom. Therefore we can say that within the VCA method averaging behaviour of the Born effective charge occurs. In fact, we can expect such a result from the well averaged polarization values.

Our results for PT are a little different from the previous ones, because ours were obtained from the lattice constant (7.43 Bohr) optimized in this work but the latter used the experimental value (7.50 Bohr). It is useful to consider the effective charges in the perpendicular part (Z_{xx}, $Z_{yy} \rightarrow Z_\perp$) and parallel part ($Z_{zz} \rightarrow Z_\parallel$) with respect to the Z axis. For $Z_\perp$, it is found that the deviation from the nominal value is large for Bi ($+3 \rightarrow +5.72$) of BS, Ti ($+4 \rightarrow +6.58$) of PT and $\mathrm{O}_\perp$ (O_x and O_y) ($-2 \rightarrow -5.53, -3.03, -3.34$) of the three compounds. Meanwhile also Ti (+5.59) of PT but Sc ($+3 \rightarrow +4.47$) of BS and $\mathrm{O}_\parallel(\mathrm{O}_z)$ ($-2 \rightarrow -4.73, -4.17, -3.38$) have large values for $Z_\parallel$. From the fact that the deviation of the effective charge from the nominal ionic charge is raised by orbital hybridization (charge transfer) and through the view of the perpendicular part area where the atomic relaxations were not allowed, we can find that there exist hybridizations between Bi atom orbitals and $\mathrm{O}_\perp$ orbitals and therefore the Bi atom plays a more important role in ferroelectric instability than the Sc atom in BS, while in the case of PT, Ti and $\mathrm{O}_\perp$ atoms play such role and the Pb atom plays an assisting role. And through the parallel part, it can be concluded that the role of B site atoms and $\mathrm{O}_\parallel$ increases when the atomic relaxation is performed.

Then we calculate the elastic tensor for compounds, which is a fourth-rank tensor originally, but is reduced to a sixth-rank matrix by the Voigt notation. In the perovskite tetragonal phase ($P\bar{4}mm$ space group), there are only six independent elements. The elastic properties of BS–PT can be compared with the experimental values, except C_{44} which is much larger than the experimental value (see table 5).

In table 6, the piezoelectric response properties are shown. Here we concentrate on e_{15} and d_{15} which measure the change of polarization perpendicular to the z axis induced by

Table 5. The elastic stiffness tensor for the tetragonal phase (10^2 GPa).

	C_{11}	C_{12}	C_{13}	C_{33}	C_{44}	C_{66}
BS	2.00	0.72	0.77	0.91	0.48	0.67
BS–PT ($x = 0.5$)	2.47	0.87	0.93	0.92	1.39	0.80
PT	2.68	1.06	0.86	0.87	0.51	0.93
BS–PT ($x = 0.57$) exp.[a]	1.26	1.06	0.99	1.00	0.49	0.41
PT exp.[b]	2.37	0.90	0.70	0.60	0.69	1.04
PT calc.[b]	1.33	0.85	0.89	0.93	0.80	0.93

[a] Reference [19].
[b] Reference [20].

Table 6. The piezoelectric tensor for the tetragonal phase where 'strain' means piezoelectric strain tensor and 'stress' means piezoelectric stress tensor.

	Strain (C m^{-2})			Stress (pC N^{-1})		
	e_{15}	e_{31}	e_{33}	d_{15}	d_{31}	d_{33}
BS	1.64	−0.68	−1.38	34.18	3.43	−20.93
BS–PT ($x = 0.5$)	13.72	−0.94	−3.05	98.53	15.12	−64.08
PT	5.68	1.61	4.44	111.30	−13.33	77.06
BS–PT ($x = 0.57$) exp.[a]	16	−6.6	13.6	330	−550	1150
BS–PT ($x = 0.7$) calc.[b]	7.25			168		
PT calc.[c]	5.65	1.87	3.68			
PT exp.[d]	4.4	2.1	5.0	53	−4.4	51

[a] Reference [19].
[b] Reference [17].
[c] Reference [21].
[d] Reference [20].

shear strain and stress. In our case e_{15} (13.72 C m^{-2}) is much closer to the experimental value (16 C m^{-2}) than the previous one (7.25 C m^{-2}) and also d_{15} is sufficiently large. If we perform the calculation at MPB ($x \approx 0.67$), we think that the result will be even closer to the experimental value but in this work it is sufficient. Anyway we can conclude that the piezoelectric response property of BS–PT is good at least as regards the shear strain, compared with that of PZT ($e_{15} = 7.58$ C m^{-2}).

4. Summary and discussion

In this work, we proposed an efficient VCA approach applicable for treating heterovalent atoms and investigated the overall material properties of perovskite ferroelectrics such as BS, PT and their solid solution BS–PT. The material properties include the electronic properties (band structure, partial DOS, and valence electronic charge density), structural properties (equilibrium cubic lattice constant, tetragonal lattice parameters with the relaxation of the atomic positions) and physical tensors (Born effective charge tensors, spontaneous polarization, elastic tensors and piezoelectric tensors). Most of the results are reasonably good as compared with the previous results and the experimental values.

Vegard's law was well satisfied as regards the cubic lattice constants. Moreover, our value of the tetragonal lattice ratio agreed with the value from the supercell method although it was still far away from the experimental value. Such agreement with the supercell method was also observed for the spontaneous polarization of the compounds. As regards the electronic

properties, it is concluded that the behaviour of the solid solution is generally well averaged from the parent compounds, except for the band gaps. Also the calculated elastic and piezoelectric tensors are reasonable compared with the experimental values, except for some elements. As regards the piezoelectric properties, more careful consideration is necessary.

Comparing with the previous results, it is emphasized that we obtain better values for the tetragonal lattice ratio and the spontaneous polarization, namely, our calculated values are much closer to the supercell method ones than the previous ones. Moreover our approach can perform direct calculations and analysis of the electronic properties of the solid solutions, while with the previous method it is not possible to do that because of the additional 'ghost' atoms. We consider that this approach could be applied to wide ranges of alloys and solid solutions without any complicated process and with reasonable results.

Acknowledgments

One of the authors (Yu) would like to thank the Gottlieb Daimler and Karl Benz Foundation for financial support, and Professors A Rappe and M Mikami for valuable discussion.

Appendix

In this appendix, we show how to transform semi-local pseudopotentials into fully nonlocal pseudopotentials by using an orthonormalized complete set of projection functions.

The semi-local pseudopotential operator can be written as follows:

$$\widehat{V}_{\mathrm{nl}}^{\mathrm{semi}} = \sum_{l=0}^{l_{\max}} \sum_{m=-l}^{l} |Y_{lm}\rangle \Delta V_l(r) \langle Y_{lm}| \tag{A.1}$$

where we do not consider the local parts because they are the same for the semi-local and nonlocal formalisms. Then, the matrix element in momentum space is as follows:

$$V_{\mathrm{nl}}^{\mathrm{semi}}(\mathbf{K}, \mathbf{K}') = \sum_{lm} \int_0^\infty \mathrm{d}r\ r^2 \langle \mathbf{K}|Y_{lm}\rangle_{\hat{\mathbf{r}}} \Delta V_l(r) \langle Y_{lm}|\mathbf{K}'\rangle_{\hat{\mathbf{r}}'} \tag{A.2}$$

where $\hat{\mathbf{r}}$ and $\hat{\mathbf{r}}'$ are the angular coordinates of position vectors $\mathbf{r}$ and $\mathbf{r}'$, respectively.

Any orthonormalized and complete basis set,

$$\sum_i |\alpha_i\rangle\langle\alpha_i| = 1, \qquad \langle\alpha_i|\alpha_j\rangle = \delta_{ij}, \tag{A.3}$$

can be put into (A.2), and then the matrix element can be divided as follows:

$$\begin{aligned} V_{\mathrm{nl}}^{\mathrm{KB}}(\mathbf{K}, \mathbf{K}') &= \sum_{lm} \int_0^\infty \mathrm{d}r\ r^2 \left(\sum_i \langle \mathbf{K}|\alpha_i\rangle \langle\alpha_i|Y_{lm}\rangle_{\hat{\mathbf{r}}} \Delta V_l(r) \sum_j \langle Y_{lm}|\alpha_j\rangle_{\hat{\mathbf{r}}'} \langle\alpha_j|\mathbf{K}'\rangle \right) \\ &= \sum_{ij} \sum_{lm} \langle \mathbf{K}|\alpha_i\rangle \left[\int_0^\infty \mathrm{d}r\ r^2 \alpha_i^{lm}(r) \Delta V_l(r) \alpha_j^{lm}(r) \right] \langle\alpha_j|\mathbf{K}'\rangle \\ &= \sum_{ij} \sum_{lm} \langle \mathbf{K}|\alpha_i\rangle \Delta V_{ij}^{lm} \langle\alpha_j|\mathbf{K}'\rangle \\ &= \sum_{ij} \langle \mathbf{K}|\alpha_i\rangle V_{ij} \langle\alpha_j|\mathbf{K}'\rangle \end{aligned} \tag{A.4}$$

where $\alpha_i(\mathbf{r}) = \sum_{lm} \alpha_i^{lm}(r) Y_{lm}(\hat{\mathbf{r}})$ and $\Delta V_{ij}^{lm} = \int_0^\infty \mathrm{d}r\ r^2 \alpha_i^{lm}(r) \Delta V_l(r) \alpha_j^{lm}(r)$.

References

[1] Ramer N J and Rappe A M 2000 *J. Phys. Chem. Solids* **61** 315–20
Ramer N J and Rappe A M 2000 *Phys. Rev.* B **62** R743–6 (Rapid Comm.)
[2] Ghosez Ph, Desquesnes D, Gonze X and Rabe K M 2000 *Fundamental Physics of Ferroelectrics 2000: Aspen Center for Physics Winter Workshop (Aspen, CO)*; *AIP Conf. Proc.* **535** 102–10
[3] Bellaiche L and Vanderbilt D 2000 *Phys. Rev.* B **61** 7877
[4] Kleinman L and Bylander D M 1982 *Phys. Rev. Lett.* **48** 1425–8
[5] Bylander D M and Kleinman L 1990 *Phys. Rev.* B **41** 907–12
[6] Fuchs M and Scheffler M 1999 *Comput. Phys. Commun.* **119** 67–98
[7] Troullier N and Martins J L 1991 *Phys. Rev.* B **43** 1993–2006
[8] Bachelet G B, Hamann D R and Schlüter M 1982 *Phys. Rev.* B **26** 4199–228
[9] Rappe A M, Rabe K M, Kaxiras E and Joannopoulos J D 1990 *Phys. Rev.* B **41** 1227–30
[10] Ramer N J and Rappe A M 1999 *Phys. Rev.* B **59** 12471–8
[11] Hartwigsen C, Goedecker S and Hutter J 1998 *Phys. Rev.* B **58** 3641–62
[12] Gonze X, Stumpf R and Scheffler M 1991 *Phys. Rev.* B **44** 8503–13
[13] Gonze X, Vigneron J P and Michenaud J-P 1989 *J. Phys.: Condens. Matter* **1** 525–40
[14] Allan D C and Teter M P 1987 *Phys. Rev. Lett.* **59** 1136–9
[15] Blöchel P E 1990 *Phys. Rev.* B **41** 5414–6
[16] Vanderbilt D 1990 *Phys. Rev.* B **41** 7892
[17] Íñiguez J, Vanderbilt D and Bellaiche L 2003 *Phys. Rev.* B **67** 224107
[18] Wen H, Wang X and Li L 2006 *J. Am. Ceram. Soc.* **89[7]** 2345
[19] Zhang S, Randall C A and Shrout T R 2004 *J. Appl. Phys.* **95** 4291
Zhang S, Randall C A and Shrout T R 2003 *Appl. Phys. Lett.* **83** 3150
[20] Kalinichen A G *et al* 1997 *J. Mater. Res.* **12** 2623
[21] Sághi-Szabó G, Cohen R E and Krakauer H 1998 *Phys. Rev. Lett.* **80** 4321
[22] Sökeland F, Rohlfing M, Krüger P and Pollman J 2003 *Phys. Rev.* B **68** 075203
[23] Perdew J P and Zunger A 1981 *Phys. Rev.* B **23** 5048
[24] Gonze X *et al* 2002 *Comput. Mater. Sci.* **25** 478–92
Gonze X *et al* 2005 *Z. Kristallogr.* **220** 558–62
[25] Hamann D R, Wu X, Rabe K M and Vanderbilt D 2005 *Phys. Rev.* B **71** 035117 and references therein